INSTITUTE OF PHYSICS PUBLISHING SEMICONDUCTOR SCIENCE AND TECHNOLOGY
Semicond. Sci. Technol. **17** (2002) 785–796 PII: S0268-1242(02)37906-9

Ion beam synthesis and n-type doping of group III–N_x–V_{1-x} alloys

K M Yu

Electronic Materials Program, Materials Sciences Division, Lawrence Berkeley National Laboratory, Berkeley, CA 94720, USA

Received 22 January 2002
Published 10 July 2002
Online at stacks.iop.org/SST/17/785

Abstract

Investigations on the synthesis of group III–N_x–V_{1-x} alloy including GaN_xAs_{1-x}, InN_xP_{1-x} and $Al_yGa_{1-y}N_xAs_{1-x}$ using N ion implantation followed by rapid thermal annealing are reviewed. The fundamental band-gap energy for the ion beam synthesized III–N_x–V_{1-x} alloys is found to decrease with increasing N-implantation dose and can be quantitatively described by the anticrossing interaction between the localized N-states and the extended states of the semiconductor matrix. N activation efficiencies in these N ion synthesized alloy films are found to be low, ∼10% for GaN_xAs_{1-x} and ∼20% for InN_xP_{1-x}. A preliminary study showed that using pulsed laser melting followed by rapid thermal annealing greatly enhanced the N activation efficiency (∼50%) in N-implanted GaAs. The N-induced conduction band modification also results in an enhancement of the maximum free electron concentration in GaN_xAs_{1-x}. A maximum free electron concentration as high as 7×10^{19} cm^{-3} was observed in heavily Se-doped $Ga_{1-3x}In_{3x}N_xAs_{1-x}$ ($x = 0.033$) films, more than 20 times larger than that observed in GaAs films grown under similar conditions. A similar increase in free electron concentration was also achieved in a S-implanted GaN_xAs_{1-x} thin film. Combining the ion synthesis of diluted nitrides and S implantation doping techniques, we realized a large increase in the electrical activation of S co-implanted with N in GaAs within a thin near-surface region (∼500 Å), indicating the formation of a heavily doped thin diluted GaN_xAs_{1-x} alloy layer with $x \sim 0.3\%$. This result has important practical implications on the fabrication of low-resistance, non-alloyed ohmic contacts to n-type GaAs.

Introduction

In conventional III–V and II–VI ternary (e.g. $In_yGa_{1-y}As$, $GaAs_{1-x}P_x$, $Cd_{1-y}Zn_yTe$) and quaternary (e.g. $In_yGa_{1-y}As_{1-x}P_x$) alloys, a fair amount (several to tens of mole fraction) of either cations and/or anions are substituted by another element in the same column of the periodic table. The physical, electronic and optical properties of these conventional alloys can be estimated by a linear interpolation between those of the end point compounds with only a slight deviation, as predicted by the virtual crystal approximation. There are also alloys in which the variation of the band gap (and subsequently other crystal properties) from one end member to the other first shows a significant decrease before increasing finally to the band gap of the other end member. This behaviour is referred to as band-gap bowing.

In recent years we witnessed the emergence of a new class of semiconductor alloys, the highly mismatched alloys (HMAs) which exhibit an unusually large band-gap bowing. In these HMAs only a small amount of more electronegative elements (typically from less than 1% to several%) substituting the metallic anion of the III–V or II–VI matrix semiconductors results in large modification in the conduction band structure of the alloys. A most notable and well studied example is the GaN_xAs_{1-x} HMA, in which strong band-gap bowing by as much as 180 meV per mole per cent of N (i.e. for $x = 0.01$) has been observed [1–3]. Comparably large band-gap reductions have also been observed in other III–N_x–V_{1-x} alloys such as GaInNAs [2, 4], GaNP [5, 6], InNP [7]

and AlGaNAs. [8, 9] The strong dependence of the band gap on the N content has made these diluted III–V nitrides important materials for a variety of applications, including long wavelength optoelectronic devices [10, 11] and high-efficiency hybrid solar cells [12, 13].

Several theoretical studies have addressed the unusually strong dependence of the fundamental gap on the N content in the group III–N–V alloys[1]. The observation of an additional feature above the fundamental gap in the optical spectrum of GaInNAs alloys [14–16] as well as the unusual pressure dependence of these transitions led to the development of a band anticrossing model (BAC) to explain the conduction band modification due to the presence of N in these alloys. In this BAC model, an anticrossing interaction between localized N-states and extended states of the host semiconductor matrix splits the conduction band into two subbands [14, 17]. The downward shift of the lower subband is responsible for the reduction of the fundamental band gap, and optical transitions from the valence band to the upper subband account for the high-energy edge. The model has been successfully used to quantitatively describe the dependencies of the upper and lower subband energies on hydrostatic pressure and on N content of $Ga_{1-y}In_yN_xAs_{1-x}$, $Ga_{1-y}Al_yN_xAs_{1-x}$, InN_xP_{1-x} and GaN_xP_{1-x} alloys [8, 14, 17–20].

In the BAC model, the dispersion relations for the upper and lower conduction subbands are given by

$$E_{\pm}(k) = \tfrac{1}{2}\left[E_{\mathrm{N}} + E_{\mathrm{M}}(k) \pm \sqrt{(E_{\mathrm{N}} - E_{\mathrm{M}}(k))^2 + 4C_{\mathrm{NM}}^2 x}\right] \tag{1}$$

where E_{N} is the energy of the N level, $E_{\mathrm{M}}(k)$ is the dispersion relation for the host semiconductor matrix and C_{NM} is the matrix element describing the coupling between N-states and extended states. For GaN_xAs_{1-x}, the downward shift of the lower subband E_- can account well for the reduction of the fundamental band gap using a value of $E_{\mathrm{N}} = 1.65$ eV above the valence band maximum derived from PL measurements in N-doped GaAs [21] and $C_{\mathrm{NM}} = 2.7$ eV from fitting the band-gap variation data with N content [14, 17].

At present, growth of III–N_x–V_{1-x} alloys is still considered challenging; bulk material has not been reported. To date most reports on III–N_x–V_{1-x} alloys involve thin films grown by gas-source molecular beam epitaxy (MBE) or metallorganic chemical vapour deposition (MOCVD) techniques. Pulse laser ablation of GaAs in NH_3 atmosphere and laser nitridation of GaAs are potential alternative methods for the formation of thin films of GaN_xAs_{1-x} [22, 23]. In this context, because only a small amount of N (<1%) can lead to a large reduction in the energy band gap of III–N_x–V_{1-x} materials, ion implantation is an attractive and feasible alternative approach to synthesize these alloys. In the first part of this paper we review our efforts in the synthesis of GaN_xAs_{1-x}, InN_xP_{1-x} and $Al_yGa_{1-y}N_xAs_{1-x}$ alloy thin films by N ion implantation [9, 20, 24–27].

As mentioned earlier, the BAC model predicts that the incorporation of small amounts of N ($\geqslant$0.1%) in GaAs leads to a large distortion of the conduction band structure. Two important aspects of this N-induced conduction band distortions are (1) the formation of the lower subband E_- that causes the band-gap energy reduction and (2) the considerable flattening of the lower subband near its minimum leading to a large increase of the electron effective mass [17, 28]. Both of these effects are expected to have significant consequences on the transport properties of these alloys [17]. In particular, it was proposed that the N-induced conduction band modifications in GaAs can be utilized to overcome the n-type doping limit in GaAs [17].

In most semiconductors, it has been well known that there exists a limitation on the maximum attainable free electron and/or hole concentrations. This limitation in most cases hinders the functionality of the semiconductor devices. The mechanism leading to free carrier limitations has been extensively studied [29–32]. A universal rule that predicts the maximum free carrier concentration achievable by doping has been developed and shown to be valid for a wide variety of semiconductor materials [33–36]. The rule is based on the amphoteric native defect model that relates the type and concentrations of compensating native defects responsible for dopant compensation to the location of the Fermi level with respect to a common energy reference, the Fermi level stabilization energy, E_{FS}. Semiconductor materials with the conduction (valence) band located close to E_{FS} can be easily doped n-type (p-type). GaAs has its conduction band at E_{FS} + 0.9 eV and its valence band at E_{FS} − 0.5 eV and thus is predicted to exhibit limitations on the maximum free electron concentration but no significant limitation on the maximum hole concentration. Experimentally, the maximum free electron concentration $n_{\max}$ in GaAs achievable under equilibrium condition is limited to about 10^{18}–10^{19} cm^{-3} [35]. This concentration corresponds to the Fermi energy located approximately at 0.1 eV above the conduction band edge or at 1 eV above E_{FS}. The amphoteric native defect model further predicts that this maximum energy location of the Fermi energy, measured relative to E_{FS}, is very similar for all group III–V semiconductors.

In the second part of this paper we review our work on the n-type doping of GaN_xAs_{1-x} alloys doped heavily with Se and S via MOCVD growth or ion implantation methods [26, 27, 36–38]. The effects of the N-induced conduction band modifications on the maximum free electron concentration in GaN_xAs_{1-x} as well as the implications on device fabrication will be discussed.

1. Ion beam synthesis of III–N_x–V_{1-x} highly mismatched alloys

The details of the N implantation conditions in the various substrate materials for the formation of III–N_x–V_{1-x} HMAs can be found in [25]. Briefly, nitrogen ions were implanted into bulk GaAs and InP crystals and MOCVD-grown 0.3–0.5 μm thick $Al_yGa_{1-y}As$ epitaxial films on GaAs substrates with AlAs mole fraction y ranging from 0.27 to 0.61. The N^+-implantations were carried out with multiple energies at room temperature, creating ~2000–3500 Å thick layers with roughly uniform N atomic concentration. The N dose was varied to obtain diluted nitride layers with implanted N concentrations corresponding to N mole fractions of

[1] For a review of the theoretical works on diluted III–V nitrides, refer to the review papers in this volume and references therein.

$x_{imp} \approx 0.008$, 0.016, 0.018, 0.02, 0.036 and 0.048. Rapid thermal annealing (RTA) was performed on the implanted samples in a flowing N_2 ambient in the temperature range of 560–950 °C for 5–120 s with the sample surface protected by either a blank GaAs or InP wafer.

It is important to recognize that only a fraction of the implanted N will become 'active' by occupying column V sublattice sites after annealing. These 'active' N atoms will be referred to as N in the group V sublattice N_V: e.g., N_{As} for GaAs and N_P for InP. The mole fraction of substitutional N in the group V sublattice will be referred to as x_{act}. The activation efficiency is then defined as the ratio of substitutional N in the group V sublattice and the total implanted N, x_{act}/x_{imp}.

Band gaps of the synthesized alloys were measured using photomodulated reflectance (PR) spectroscopy at room temperature. Radiation from a 300 W halogen tungsten lamp dispersed by a 0.5 m monochromator was focused on the samples as a probe beam (∼1 mm beam size). A chopped HeCd laser beam ($\lambda = 4420$ Å or 3250 Å) provided the photomodulation. PR signals were detected by a Si photodiode using a phase-sensitive lock-in amplification system. The values of the band gap and the linewidth broadening were determined by fitting the PR spectra to the Aspnes third-derivative functional form [39].

1.1. GaN_xAs_{1-x}

Channelling Rutherford backscattering (c-RBS) measurements revealed that all as-implanted GaAs samples are highly damaged yet crystalline. The high dechannelling and the absence of direct scattering peak in the c-RBS spectra suggest that majority of the damage present in the top 300 nm layer of the sample consists of extended crystalline defects. No optical transition can be observed in the PR spectra from N^+-implanted GaAs samples after RTA at temperatures lower than 750 °C, most likely due to the poor crystalline quality of the samples.

Figure 1 shows the PR spectra from an unimplanted GaAs and a series of N-implanted GaAs samples with $x_{imp} \approx$ 0.018, 0.02 and 0.036 after RTA at 800 °C for 10 s. The PR spectra shown in figure 1 exhibit well-resolved spectral features related to the fundamental band-gap transitions. The significant broadening of the features in the implanted samples can be attributed mainly to the tails in the distribution of N and remaining post-implantation damage [9]. Clearly, the band-gap reduction ΔE is a direct result of the formation of GaN_xAs_{1-x} alloy layers and increases with implantation dose in a way analogous to the reduction of the fundamental band-gap energy in GaN_xAs_{1-x} alloys with increasing N content. The mole fraction of 'active' N, x_{act}, in these ion beam synthesized GaN_xAs_{1-x} layers was derived from the observed ΔE values by using the band anticrossing model (equation (1)) and is shown in the inset of figure 1. An activation efficiency of about 10–15% has been achieved for $x_{imp} < 0.036$. The highest x_{act} achieved is ≈0.004 for an implanted N $x_{imp} \approx 0.036$.

Figure 2 shows the band-gap reduction ΔE from a series of N^+-implanted GaAs samples with $x_{imp} \approx 0.02$ subjected to RTA at temperatures between 725 and 870 °C. ΔE decreases as the RTA temperature increases, especially above 800 °C. In

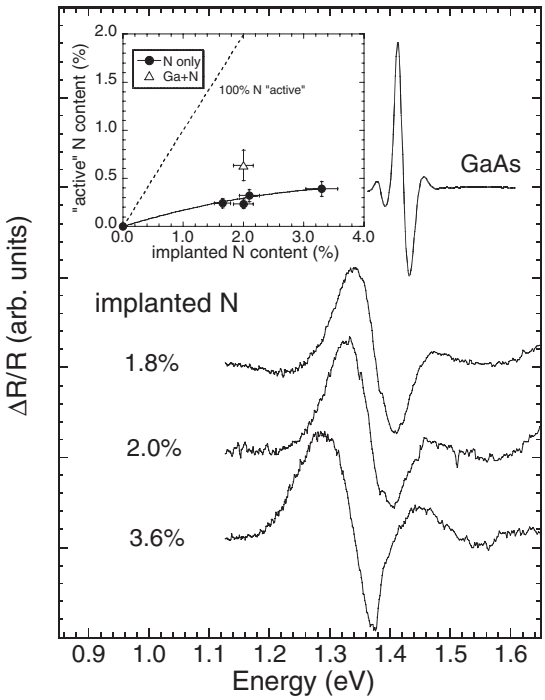

Figure 1. A series of PR spectra from N-implanted GaAs with implanted N doses to 1.8, 2.0 and 3.6% after 10 s RTA at 800 °C. The inset shows the mole fraction of N incorporated in the As sublattice calculated from the band-gap reduction as observed by the PR measurements using equation (1).

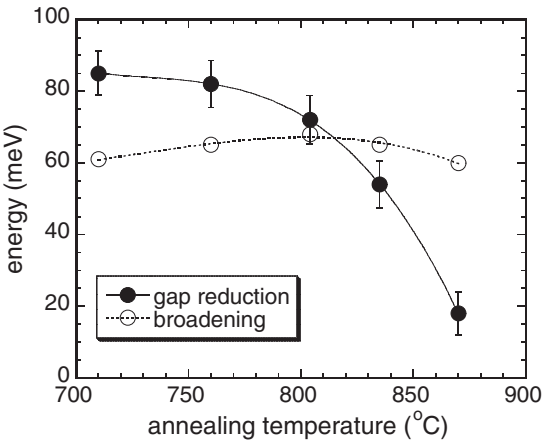

Figure 2. The band-gap reduction (solid circles) and the lineshape broadening (open circles) from the PR spectra from N-implanted GaAs samples with $x_{imp} \approx 0.02$ as a function of RTA temperature.

fact, only a negligible band-gap reduction ΔE (∼10 meV) was observed when the RTA temperature was raised to above 870 °C, indicating that less than 0.1% of N remained substitutional in the As sublattice. SIMS measurements showed that the N did not diffuse out of the implanted region even after RTA at 900 °C for 20 s. The results indicate that the substitutional configuration of the N_{As} is thermally unstable.

Transmission electron micrographs (TEMs) obtained for N- and N+Ga-implanted GaAs samples after RTA at 800 °C for 10 s are shown in figure 3. In addition to typical implantation-induced defects, void-like defects were also present in both samples. In the GaAs sample implanted with N only, a layer

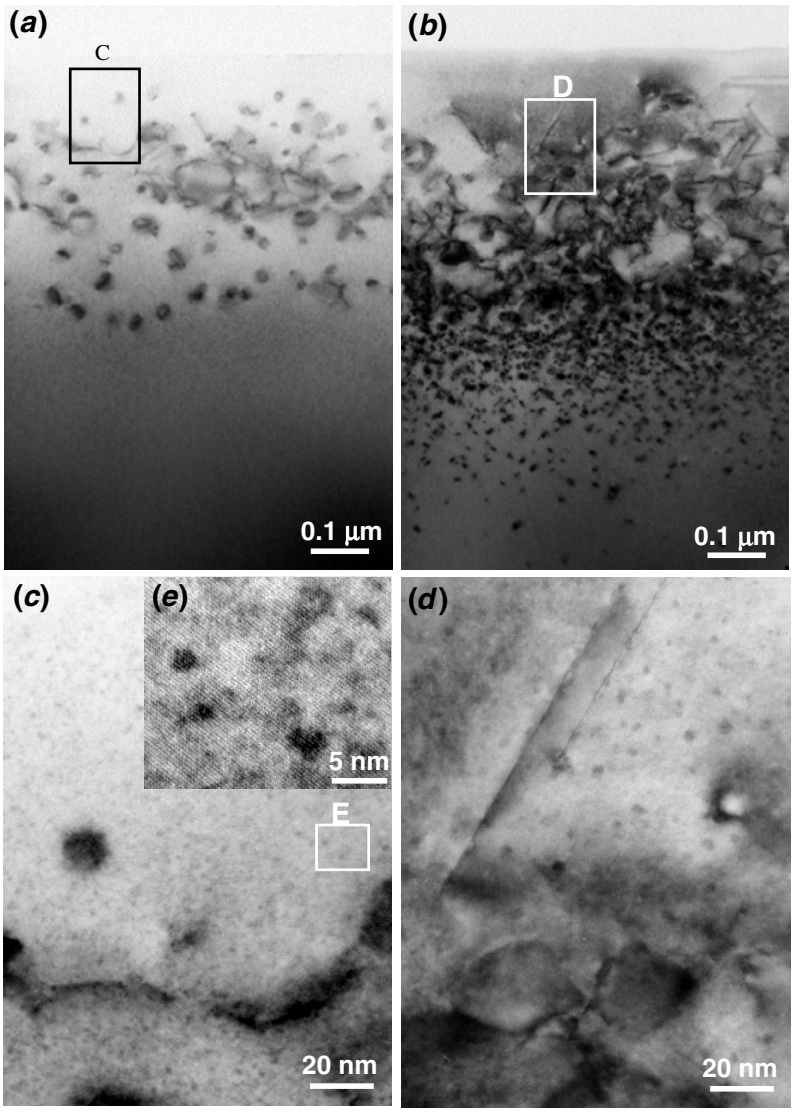

Figure 3. TEMs of GaAs-implanted with N ((*a*), (*c*) and (*e*)) and co-implanted with N and Ga ((*b*) and (*d*)).

containing a very high density of small voids, with an average size of about 2–3 nm, started forming just below the surface and continued to a depth of about 0.6–0.7 μm [26, 27]. Such void-like defects are not observed in samples implanted with S and are present only in N-implanted samples. This strongly suggests that these voids are related to N and are likely formed by the segregation of N during annealing. The formation of these voids may be the result of the presence of a high vacancy concentration in the GaAs samples due to the N-implantation. We believe that these voids (or N bubbles) may account for the low N activation efficiency in these samples.

We have also attempted to increase the activation efficiency in the N-implanted GaAs samples by Ga ion co-implantation. In many III–V semiconductors, co-implantation of a matrix element (e.g., Ga in GaAs) to restore the local stoichiometry has been used successfully to enhance incorporation of electrically active dopants on the opposite lattice sites [40–43]. In the present study, equal amount of Ga ions were co-implanted with N in GaAs in such a way that their atomic profiles overlapped.

For samples after RTA under identical conditions, we observed an enhancement of more than a factor of 2 in the activation efficiency when Ga atoms were co-implanted with N in GaAs. This is apparently due to the creation of a locally non-stoichiometric (Ga-rich) region with a high concentration of As vacancies available for N substitution. After RTA at 800 °C for 10 s, with Ga co-implantation, an $x_{\mathrm{act}} \approx 0.0065$ has been achieved (see inset, figure 1). Moreover, the N_{As} in the GaN_xAs_{1-x} layers formed by Ga and N co-implantation in GaAs are thermally more stable. TEM (figure 3) results on the Ga+N co-implanted sample show that the voids are larger (with an average diameter of about 5–6 nm) but their density was much lower. They are located in a relatively narrow layer at depths between approximately 0.1 and 0.4 μm. These two effects indicate that less N is trapped in the voids and could account for the measured higher (by a factor of 2) N activation and thermal stability in the Ga+N co-implanted samples.

However, such co-implantation created a highly defective GaN_xAs_{1-x} layer due to the heavy mass of the Ga ions, as is evident in the broad linewidths in the PR spectra from the Ga+N co-implanted samples. This is also evident in the TEM

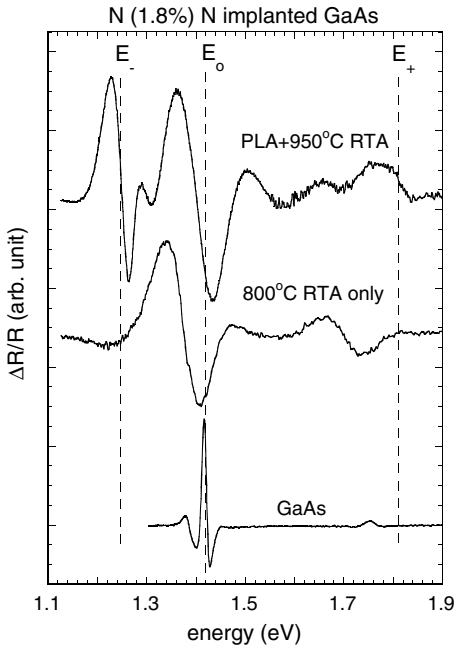

Figure 4. PR spectrum from N-implanted GaAs samples with $x_{\mathrm{imp}} \approx 0.018$ after laser and rapid thermal annealing at 950 °C (PLA+RTA) with laser pulse energy of 0.35 J cm^{-2}. PR spectra of an unimplanted GaAs and a N-implanted GaAs RTA at 800 °C only are also shown.

shown in figure 3. Therefore, the Ga co-implantation method is not a feasible way for fabricating high-quality GaN_xAs_{1-x} layers.

Recently, we have explored alternative means to improve N incorporation in N ion synthesized GaN_xAs_{1-x} alloys using the pulsed laser annealing (PLA) method [44]. The PLA technique involves the melting induced by pulsed laser of the implant-amorphized (damaged) layer and its subsequent rapid epitaxial regrowth. Epitaxy is seeded at the solid–liquid interface by the crystalline bulk in a manner very similar to liquid phase epitaxy (LPE) but with the whole process occurring on a much shorter timescale, typically between 10^{-8} and 10^{-6} s. PR measurements on the PLA samples with laser pulse fluence of 0.35 J cm^{-2} do not show any optical transition. This is consistent with the c-RBS results that show higher yields for these samples than the unimplanted sample, indicating that the regrown layer is still defective. Distinct optical transitions are observable only in the PR spectra of PLA samples after RTA at temperatures higher than 800 °C. Figure 4 shows PR spectra from the PLA + 950 °C RTA sample with laser pulse fluence of 0.35 J cm^{-2} together with PR spectra from an unimplanted GaAs and a N-implanted GaAs RTA at 800 °C only. PR spectra of the PLA + RTA samples clearly exhibit a main spectral feature at 1.26 eV, which arises from a GaN_xAs_{1-x} formed via the laser melting process. Using the BAC model, the N content in the GaN_xAs_{1-x} synthesized by N-implantation and subsequent PLA+RTA is $x = 0.009$. This corresponds to a N activation efficiency of ∼50%, a factor of 5 higher than that in GaN_xAs_{1-x} thin films synthesized by N-implantation and RTA only. The corresponding upper subband E_+ of this GaN_xAs_{1-x} layer is also calculated and is ≈1.81 eV. This high-energy transition is clearly observed in our PLA+RTA ($T \geqslant 900$ °C) samples as indicated in figure 4.

Another prominent feature is observed around 1.4 eV in the PR spectra of the PLA+RTA samples. This transition exhibits a slight blueshift from 1.36 to 1.4 eV as the RTA temperature increases from 800 °C to 950 °C. Since the N^+-implanted GaAs region is ∼300 nm thick and the LPE-regrown region with LA fluence of 0.35 J cm^{-2} is estimated from c-RBS to be only ∼100 nm, the underlying N containing layer is expected to be similar to samples after RTA only. Indeed, the broad lineshape and the position of this transition are similar to those from a GaN_xAs_{1-x} layer formed by RTA alone.

Furthermore, the substitutional N_{As} appear to be thermally more stable in the PLA layer. It can be argued that the laser melting results in a complete local rearrangement of the atom sites leading to the formation of strong Ga–N bonds stabilizing N atoms on the anion sites. The subsequent, lower temperature RTA cannot break these bonds but improves the overall crystal quality by an atomic diffusion and rearrangement of the lower energy defects. We should point out that N_{As} in the MOCVD-grown GaN_xAs_{1-x} layers are also found to be thermally stable at an annealing temperature of 950 °C [44].

1.2. InN_xP_{1-x}

Large band-gap reductions in diluted InN_xP_{1-x} alloys grown by gas source molecular beam epitaxy (GSMBE), similar to those found in GaN_xAs_{1-x}, were reported by Bi and Tu [7]. However, while GaN_xAs_{1-x} films with x up to 0.05 have been grown by both MOCVD or MBE techniques, the maximum N concentration achieved to date in the InN_xP_{1-x} system is 0.009 [7]. The low N incorporation into InP was attributed to the very high equilibrium N_2 vapour pressure over InN and the relatively weak In–N bond strength compared to that of InP.

The optical transitions from InN_xP_{1-x} formed by N^+-implantation with increasing N dose in InP after RTA at 800 °C for 10 s are shown in figure 5. A monotonic decrease in the band gap is observed as the implanted N dose increases. For the highest implanted N dose corresponding to $x_{\mathrm{imp}} \approx 0.048$, the band gap is estimated to be 1.17 eV, corresponding to $\Delta E = 180$ meV with reference to an unimplanted InP sample ($E_{\mathrm{g}} = 1.35$ eV).

We found that the experimental band-gap energies for epitaxial InN_xP_{1-x} thin films grown by the GSMBE method can be best described using the BAC model (equation (1)) with a coupling matrix element $C_{\mathrm{NM}} = 3.5$ eV [20]. Using this fitted parameter, we calculated the x_{act} in InN_xP_{1-x} layers formed by N^+-implantation from the ΔE values obtained by the PR measurements; the results are presented in the inset of figure 5. The amount of N incorporated on the P sublattice N_P in the InN_xP_{1-x} layers is $x_{\mathrm{act}} = 0.005$, 0.0065 and 0.012 for samples implanted with $x_{\mathrm{imp}} \approx 0.008$, 0.016 and 0.048, respectively. Note that the maximum value achieved for x, 0.012, exceeds that reported to date ($x = 0.009$) [7] for InN_xP_{1-x} thin films grown by the GSMBE technique. For the N-implantation dose corresponding to x_{imp} in the range of 0.01–0.02, the activation efficiency is ∼40%, much higher than that in N^+-implanted and RTA GaAs.

Unlike in the GaN_xAs_{1-x} layers synthesized by N^+-implantation and subsequent RTA in GaAs mentioned above, where we have found that the configuration with N

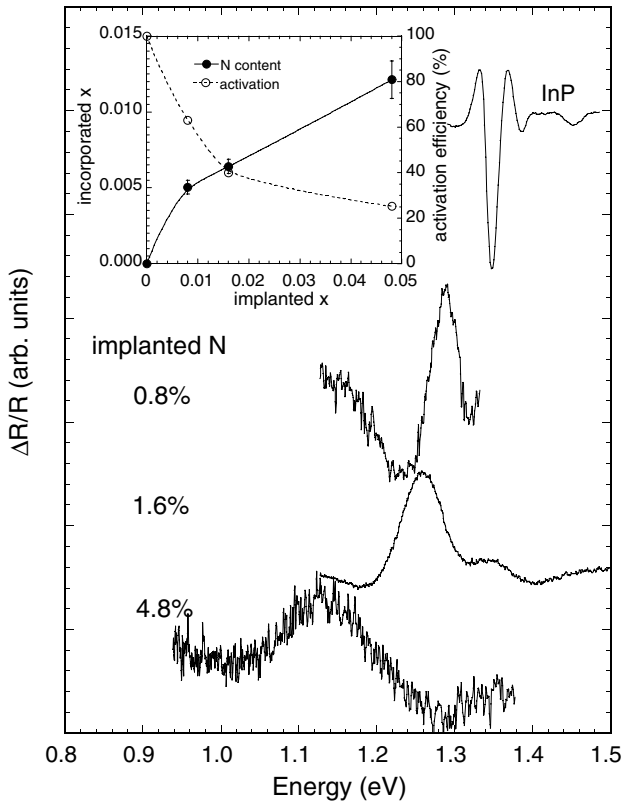

Figure 5. The PR spectra from N-implanted InP with $x_{\rm imp} \approx 0.008$, 0.016 and 0.048 after 10 s RTA at 800 °C. The inset shows the mole fraction of N incorporated on the P sublattice calculated from the band-gap reduction using the band anticrossing model. The activation efficiencies of N in the three cases are also plotted.

atoms substituting As sites is thermally unstable, the N atoms in the P sublattice of the InN_xP_{1-x} layers are thermally stable. Only a small decrease in ΔE (<20 meV) is observed for the highest annealing temperature used in this study (850 °C). The high activation efficiency and the good thermal stability of N in InP may be due to the smaller size difference between the N and P atoms compared to that between the N and As atoms.

Figure 6 shows a PR spectrum from a N-implanted InP sample with $x_{\rm imp} \approx 0.016$ after RTA at 800 °C for 10 s ($x_{\rm act} \approx 0.0065$) taken over a wide photon energy range (1.1–2.3 eV). A weak feature in the PR spectrum corresponding to the optical transition associated with the E_+ edge is clearly observable at 2.1 eV. This transition corresponds to an energy shift from the localized N-states $E_+ - E_{\rm N} = 100$ meV, in perfect agreement with the downward energy shift $E_{\rm M} - E_- = 100$ meV for this sample. This again confirms that the BAC model provides a quantitative description for the N-induced modifications in the conduction band of the III–N_x–V_{1-x} alloy system.

1.3. $Al_yGa_{1-y}N_xAs_{1-x}$

Similar to the case of N^+-implanted GaAs, we also observe a significant N-induced reduction of the band gap in N^+-implanted Al_yGa_{1-y} As thin films [8, 24, 25]. Figure 7 shows a series of PR spectra from Al_yGa_{1-y}As samples with increasing AlAs mole fraction implanted with N ($x_{\rm imp} \approx 0.018$) after RTA at 800 °C for 10 s (solid lines) together with the spectra of the as-grown materials (dotted lines). The values of the optical

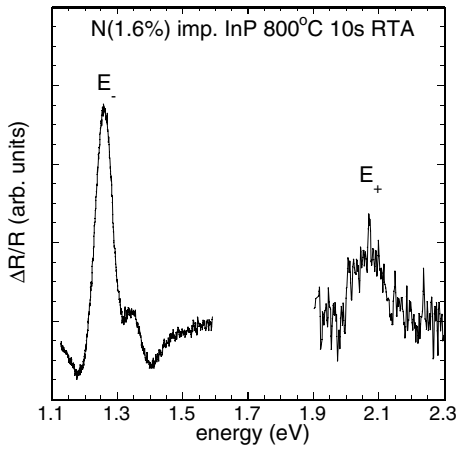

Figure 6. A PR spectrum from a N-implanted InP sample with $x_{\rm imp} \approx 0.016$ after RTA at 800 °C for 10 s taken over a wide photon energy range showing both the E_- and E_+ transitions.

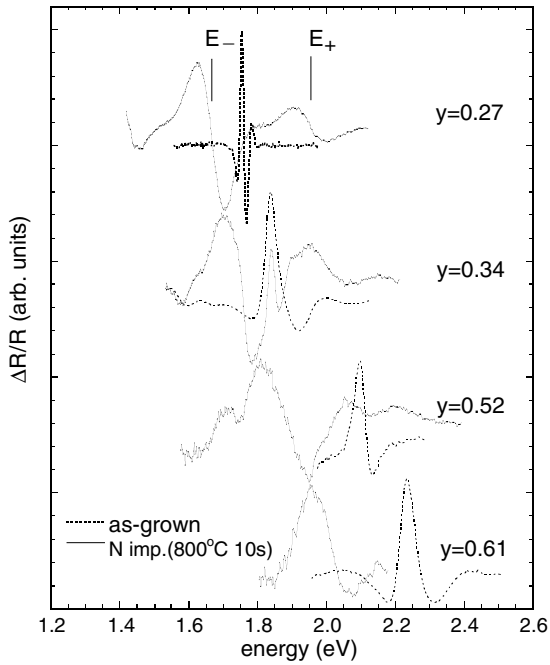

Figure 7. A series of PR spectra from Al_yGa_{1-y} As samples with various AlAs mole fractions implanted with N ($x_{\rm imp} \approx 0.018$) after RTA at 800 °C for 10 s (sold lines) together with the spectra of the as-grown materials (dotted lines).

transitions from the valance band to the lower E_- and upper E_+ subbands for $Al_yGa_{1-y}N_xAs_{1-x}$ formed by N^+-implantation in Al_yGa_{1-y} As samples as a function of AlAs mole fraction y as measured by PR are displayed in figure 8. The known dependencies of the Γ, L and X conduction-band minima on y are also shown in the figure. The dependence of the localized nitrogen level $E_{\rm N}$ on y has been determined from published results on N-related photoluminescence in Al_yGa_{1-y} As alloys doped with N at low impurity-like levels to be $E_{\rm N} = 1.65 + 0.58y$ (eV) and is shown by the dotted line in figure 8 [21, 45–47].

Results in figure 7 show an evolution of the E_- and E_+ energies as functions of the composition. For GaAs ($y = 0$) the wavefunction of the E_- edge consists mostly of Γ edge wavefunction. This leads to strong optical transitions from the

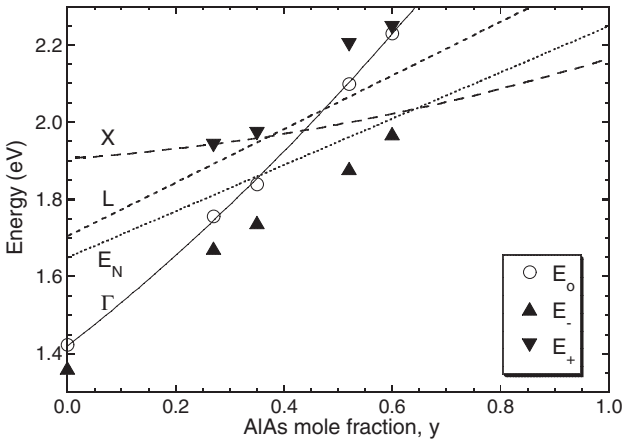

Figure 8. The E_- and E_+ transition energies measured on ion beam synthesized $Al_yGa_{1-y}N_xAs_{1-x}$ samples. The variation of E_N and the Γ, X and L conduction band edges as a function of AlAs mole fraction in Al_yGa_{1-y} As alloys are also shown.

valence band to the E_- subband. On the other hand E_+ has mostly the character of the close lying, highly localized N state that only very weakly couples optically to the extended valence band states. As is seen in figure 8, the composition dependence of the relative locations of the interacting E_N and Γ levels leads to a change in the nature of the E_+ and E_- subbands. At larger y the Γ edge moves to higher energies and the E_+ subband acquires more Γ band-like character. This is reflected in the greatly enhanced strength of the optical transitions to the E_+ subband (as seen in figure 7). At the same time E_- becomes more like localized N level with decreasing oscillator strength for optical transitions. This Al composition-induced evolution of the anticrossing interaction resembles, previously observed, change in the nature of E_+ and E_- states with hydrostatic pressure [14].

Another interesting feature of the results in figure 8 is the N-induced transformation of the nature of the fundamental band gap in $Al_yGa_{1-y}N_xAs_{1-x}$. As seen in figure 8, $Al_yGa_{1-y}As$ becomes an indirect gap semiconductor when X shifts below Γ minimum for $y > 0.44$. Consequently, no PR signal is observed for the lowest band gap for these alloy compositions. However, as is seen for the samples with $y = 0.52$ and $y = 0.61$, incorporation of a small amount of nitrogen leads to the appearance of direct gap transitions with clearly visible PR spectrum. The direct gap is associated with the transitions to E_- subband that originates from localized N-states and partially acquires Γ-like character through the interaction with the high-lying Γ band edge. This change in the nature of the fundamental band gap is exactly the same as that recently observed in GaN_xP_{1-x} alloys [6].

The active N contents in the $Al_yGa_{1-y}N_xAs_{1-x}$ layers synthesized by N^+-implantation can be estimated by equation (1) using the known composition dependence for the Γ band edge, $E_M(y)$, the localized N level, $E_N(y)$ and the measured values of E_+ and E_- in figure 8. Assuming that in $Al_yGa_{1-y}N_xAs_{1-x}$, C_{NM} does not depend on the Al composition and is equal to 2.7 eV, the mole fractions of active nitrogen in $Al_yGa_{1-y}N_xAs_{1-x}$ are ∼0.002–0.003. This corresponds to an activation efficiency in the range of 10% –16%.

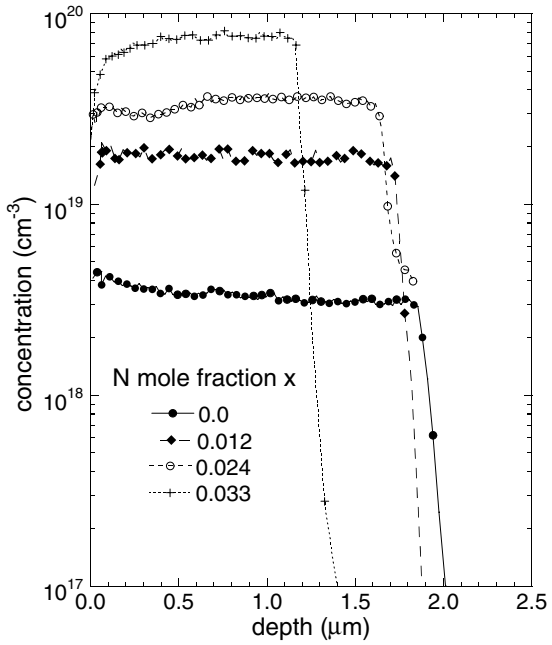

Figure 9. Free electron concentration profiles for the $Ga_{1-3x}In_{3x}N_xAs_{1-x}$ alloy films with $x = 0$–0.033 measured by the ECV technique.

2. Nitrogen-induced enhancement in maximum electron concentration

The BAC model predicts that the N-induced modifications of the conduction band of the III–N_x–V_{1-x} alloys would have profound effects on their transport properties [17]. In the following sections we review our work on the n-type doping of GaN_xAs_{1-x} materials with dopants incorporated in the alloys either during growth [36] or via ion implantation after growth [37]. Finally, we describe our attempt to combine both the ion beam synthesis and implantation doping techniques to form a thin layer of GaN_xAs_{1-x} alloy with free electron concentration exceeding that in GaAs and the potential of this co-implantation technique for GaAs device fabrication [38].

2.1. MOCVD-grown $Ga_{1-3x}In_{3x}As_{1-x}Nx$:Se

The details on the growth and characterization of the Se-doped $Ga_{1-3x}In_{3x}As_{1-x}N_x$ films are described in [48] and [36]. SIMS measurements show a uniform concentration of Se in the range of 2–7 × 10^{20} cm^{-3} in the $Ga_{1-3x}In_{3x}As_{1-x}N_x$ films. We note that the dimethylhydrazine used as a N source in the OMVPE growth caused hydrogen to be present in the range of 10^{19}–10^{20} cm^{-3} for all films with $x > 0$. Hydrogen could passivate shallow donors in GaAs. However, in our samples the Se dopant concentrations are always more than three times higher than the hydrogen concentrations. Profiles of the net donors for the $Ga_{1-3x}In_{3x}N_xAs_{1-x}$ films with $x =$ 0–0.033 measured by the electrochemical capacitance–voltage (ECV) technique are shown in figure 9. The ECV measured net donor concentrations on all of the $Ga_{1-3x}In_{3x}N_xAs_{1-x}$ films agree well (within 20%) with the free electron concentrations obtained by Hall effect measurements. Since the Se atomic concentrations in these films are at least an order of magnitude higher than the free electron concentration, the measured free

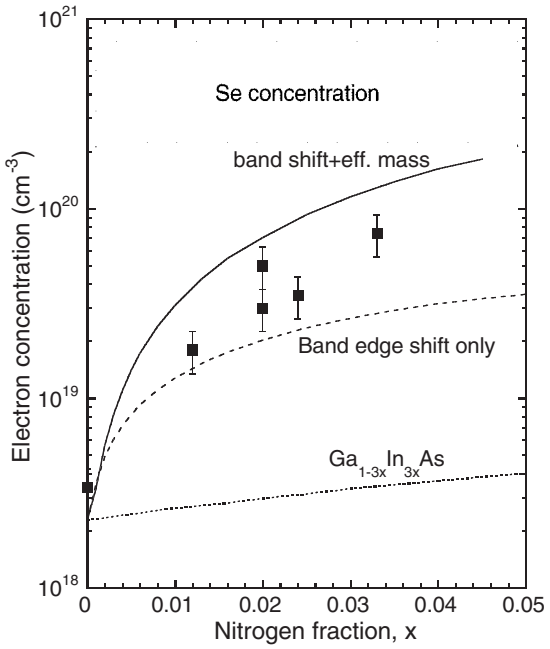

Figure 10. A comparison of the measured maximum electron concentration with the calculated values as a function of N fraction in $Ga_{1-3x}In_{3x}N_xAs_{1-x}$. Two different cases of the calculated n_{max} are shown: one included effects of downward shift of the conduction band only (dashed curve) and the other included both the band shift and the enhancement of the density of states effective mass (solid curve). The calculated n_{max} for samples with no N (i.e. the effects from the band-gap lowering produced by In incorporation only are considered) are also shown in the figure (dotted curve). The shaded area indicates the range of Se concentration in these samples.

electron concentration shown in figure 9 can be considered to be the maximum achievable free electron concentration, n_{max}, for the specific growth conditions. Figure 10 shows the graph of n_{max} obtained by ECV as a function of N content, x. The values of n_{max} increase rapidly with x with a maximum observed value of 7×10^{19} cm^{-3} for $x = 0.033$. This value is ∼20 times the value observed for a GaAs film (3.5×10^{18} cm^{-3}) grown under the same conditions.

The much-enhanced n_{max} in $Ga_{1-3x}In_{3x}N_xAs_{1-x}$ films can be explained by considering the N-induced conduction band modifications. According to the amphoteric native defect model, the maximum free electron concentration is determined by the Fermi energy which is constant with respect to the Fermi stabilization energy E_{FS} [33]. Therefore, the downward shift of the conduction band edge towards E_{FS} and the enhancement of the density of states effective mass in GaInNAs lead to a much larger concentration of uncompensated, electrically active donors for the same location of the Fermi energy relative to E_{FS}. The calculated n_{max} as a function of x for $Ga_{1-3x}In_{3x}N_xAs_{1-x}$ due to the downward shift of the conduction band caused by the level anticrossing only is shown in figure 10 as the dashed curve. Since this curve lies well below all the experimental data, it clearly indicates that the band-gap reduction alone cannot fully explain the large enhancement of the doping limits in III–N–V alloys.

The calculations of the maximum free electron concentration that include both the effects of band-gap reduction and the increase in the effective mass are shown as the solid line in figure 10. As is seen in figure 10, the theory accounts quite well for the experimentally observed increase of the electron concentration with x. We note that the predicted value of n_{max} was not reached in our films. We attribute this difference between experimental and theoretical results to the compensation and passivation of donors by N-related defects and H present in the samples. We should also mention that a recent report by Uesugi and Suemune also found an electron concentration as high as $\sim 10^{20}$ cm^{-3} in a GaAsNSe quaternary (with Se content up to 15%) thin film grown by metallorganic molecular beam epitaxy technique [49].

In addition, electron mobility in the Se-doped $Ga_{1-3x}In_{3x}N_xAs_{1-x}$ films was found to be in the range of 20–60 cm^2 V^{-1} s^{-1} from Hall effect measurements. This can be attributed to the strong alloy disorder scattering which is almost three orders of magnitude more effective than the scattering in standard semiconductor alloys, as well as to the enhanced electron effective mass in these alloys [17, 28]. These values of electron mobility in the $Ga_{1-3x}In_{3x}N_xAs_{1-x}$ alloys are to be expected from the N modified conduction band structure and are similar to those for holes in GaAs with comparable effective mass.

2.2. Implantation doping in GaN_xAs_{1-x} thin films

While Se-doped $Ga_{1-3x}In_{3x}N_xAs_{1-x}$ alloys grown by MOCVD have shown enhanced n_{max} in accordance with the BAC model, similar behaviours are also observed in a S^+-implanted GaN_xAs_{1-x} thin film [37]. In this work S ions were implanted in a MOCVD-grown GaN_xAs_{1-x} thin film (1.1 μm thick with nominal $x = 0.008$) and a semi-insulating (100) GaAs wafer (SI–GaAs) with multiple energies creating a close to uniform S atomic concentration of $\sim 4 \times 10^{19}$ cm^{-3} throughout the GaN_xAs_{1-x} layer.

Figure 11 displays the carrier concentration profiles measured by the ECV technique for the S-implanted GaN_xAs_{1-x} and SI–GaAs samples after RTA. A striking difference in the free electron concentration n measured in the SI–GaAs and GaN_xAs_{1-x} samples is observed. In the SI–GaAs sample, $n \sim 2.5 \times 10^{17}$ cm^{-3} was measured in the bulk of the implanted layer, with a higher $n \sim 5 \times 10^{17}$ cm^{-3} towards the end of the implantation profile. This region with higher electron concentration coincides with a region with net excess Ga as calculated by the Boltzmann transport equation [50]. Consequently, S substitution in the As sublattice is enhanced due to the presence of excess As vacancies. In the GaN_xAs_{1-x} sample we observed values of n as high as 6×10^{18} cm^{-3}, a factor of >20 times higher than that in SI–GaAs.

The maximum electron concentration attained by S^+-implantation in GaAs reported in the literature is $\sim 2 \times 10^{18}$ cm^{-3} with typical implantation parameters and annealing temperatures below 1000 °C [51–53], much higher than that obtained for the SI–GaAs sample in this work. This may also be due to the high-energy implantation [52] and the non-optimized RTA process. We emphasize here the direct comparison between the two samples that were processed (implanted and annealed) together in precisely the same way.

Again, we estimate the theoretical n_{max} in GaN_xAs_{1-x} due to the N-induced conduction band modification within the framework of the BAC model and the amphoteric native

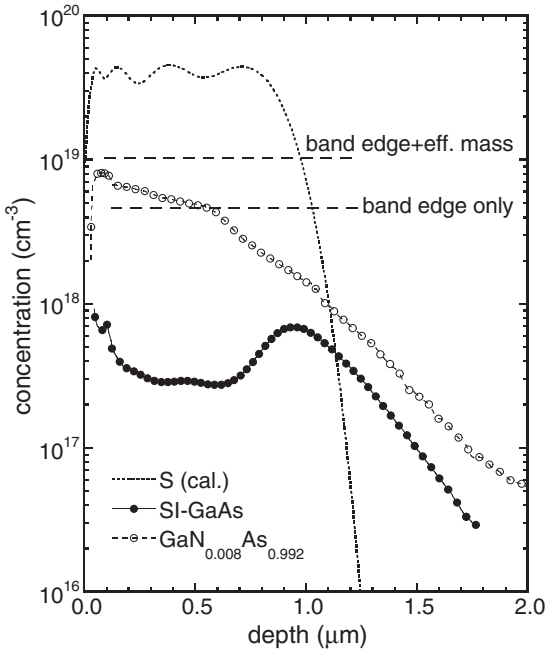

Figure 11. Ionized donor concentration profiles for the GaN_xAs_{1-x} films and the SI–GaAs standard measured by the ECV technique. The dashed horizontal lines indicate the theoretical free electron concentrations in $Ga_{1-x}N_xAs$ by considering only the effects of the downward shift of the conduction band (band edge only) and both the effects of band-gap reduction and density of states effective mass enhancement (band edge+effective mass).

defect model and obtain a $n_{max} \sim 1 \times 10^{19}$ cm^{-3} for the $GaN_{0.008}As_{0.992}$ sample [37]. This value is in a reasonably good agreement with our measured concentration of 6×10^{18} cm^{-3}. The n_{max} calculated by considering the effect of the conduction band edge shift only, assuming a constant effective mass of $0.07m_0$ (the effective mass in GaAs), is about 5×10^{18} cm^{-3}. This is a factor of 2 smaller than the n_{max} calculated when both effects were taken into account. In fact, calculations show a twofold increase of the effective mass of electrons at E_{Fmax} in the GaN_xAs_{1-x} sample.

Although the sheet electron density (n_H,) and mobility (μ_H) obtained from Hall effect measurements for the the S$^+$-implanted SI–GaAs and GaN_xAs_{1-x} samples are very similar, the ECV measured sheet electron density differs by an order of magnitude. This apparent contradiction can be resolved by recognizing that S diffuses rapidly in GaAs during RTA [51–53], creating a high-mobility, n-type GaAs layer below the low mobility, high n GaN_xAs_{1-x} films.

Using the expressions for parallel transport [54], the electron mobilities for the GaN_xAs_{1-x} layer, μ_{GaNAs}, and the S-doped substrate region, μ_{GaAs}, are extracted from the Hall and ECV data to be 110 and 2240 cm^2 V^{-1} s^{-1}, respectively. These mobility values agree well with those reported in the respective materials with similar electron concentration. The much lower electron mobility in GaN_xAs_{1-x} alloys is similar to that in Se-doped $Ga_{1-y}In_yN_xAs_{1-x}$ alloys and, as mentioned before, can be attributed to the strong alloy disorder scattering as well as to the enhanced electron effective mass in these alloys [17, 28].

We have also investigated the doping efficiency of group IV elements in GaN_xAs_{1-x} alloy films. A common group IV donor, Si, was implanted in $GaN_{0.008}As_{0.992}$ alloy films. In contrast to the S implantation, Hall effect measurements show that a high-resistivity layer was formed by Si implantation. In fact, attempts to carry out ECV profiling of the ionized donors were not successful due to the inability to form reasonable ohmic contacts to the layers. We speculate that the Si atoms have a high tendency to form Si_3N_4 precipitates during post-implantation annealing, thus rendering the Si dopants inactive. The role of Si in GaN_xAs_{1-x} alloys will be investigated further in the following section.

2.3. Doping of N$^+$-synthesized GaNAs by S-implantation

The above results showed that free electron concentrations exceeding the maximum doping limit in GaAs could be achieved in MOCVD-grown GaN_xAs_{1-x} thin films when group VI dopants (S and Se) are introduced into the films either during growth or via ion implantation. We have also demonstrated that GaN_xAs_{1-x} alloys can be formed by N$^+$-implantation in GaAs. Here we describe our efforts on the simultaneous doping and synthesis of a GaN_xAs_{1-x} thin film by co-implantation of a dopant element (either group VI (S and Se) or group IV (Si)) and N in GaAs with the goal of forming a highly n-type GaN_xAs_{1-x} layer with n_{max} exceeding that of GaAs.

N and S ions were implanted sequentially into a semi-insulating GaAs wafer at room temperature. Both species were introduced by multiple energy implantation forming a $\sim$0.35 μm thick layer with N concentrations $\sim 3.6 \times 10^{20}$ cm^{-3} with the top $\sim$0.2 μm doped having a uniform S concentration of $\sim 6.3 \times 10^{19}$ cm^{-3}. Besides S, other dopant species, Se and Si are also implanted together with N and their results are also discussed briefly.

In the GaAs sample implanted with S only and RTA at 945 °C, Hall effect measurement shows that the sheet density of free electrons is 2.5×10^{13} cm^{-2} with Hall mobility of 2200 cm^2 V^{-1} s^{-1}, corresponding to an overall activation efficiency of only 1.7%. ECV profiling of this sample reveals that although the implanted S concentration is $>6 \times 10^{19}$ cm^{-3}, the n_{max} achieved is smaller than 4×10^{18} cm^{-3}, corresponding to a maximum activation efficiency of only 6%.

Figure 12 shows a comparison of the ECV determined free electron concentration profiles for the GaAs samples implanted with S alone and co-implanted with S and N (S+N) after RTA at 945 °C for 10 s. The calculated, as-implanted S and N atomic distributions are also shown in the figure. The most striking difference in the electron concentration profiles between the S only and (S+N) samples shown in figure 12 is the much-enhanced electron concentration in the (S+N) sample in a narrow region ($\sim$500 Å) near the surface. Enhanced activation due to additional implantation damage by co-implantation of an inert element (e.g. Ar) has been observed for light dopant ions (e.g. C or Be) in GaAs and InP [41, 55, 56]. However, for heavy dopant ions (such as Zn or Ge), reduced electrical activation was observed with additional implantation damage [57]. Ion channelling experiment shows that the S-implantation in this experiment introduced sufficient damage to amorphize a layer of GaAs $\sim$3000 Å thick. Therefore, additional damage by the lighter N ions is not expected to have any positive effect in the electrical activation of the S. The much-enhanced maximum free

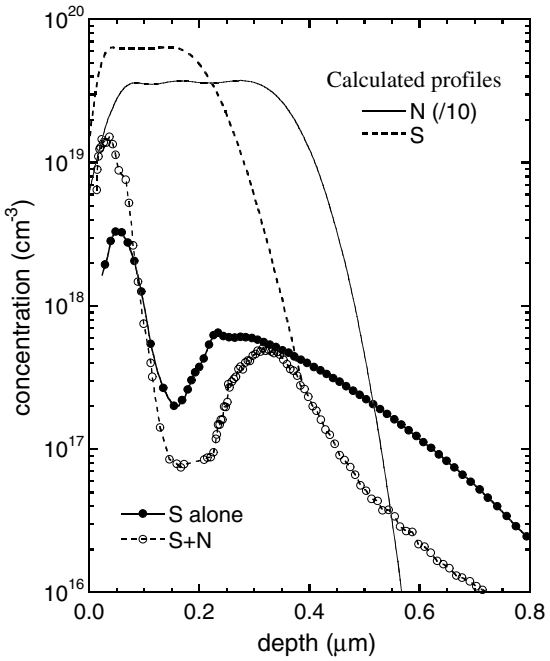

Figure 12. The ECV measured net donor concentration profiles for the GaAs samples implanted with S alone and S+N after RTA at 945 °C for 10 s. The calculated atomic profiles for both the implanted S and N are also shown.

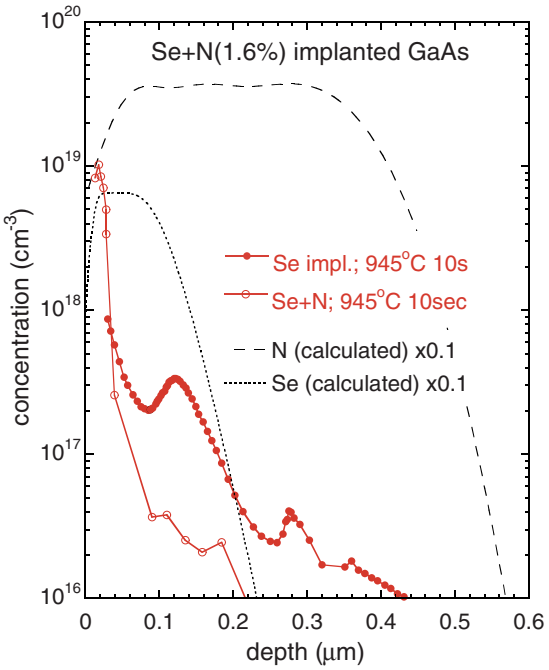

Figure 13. The ECV measured net donor concentration profiles for the GaAs samples implanted with Se alone and Se+N after RTA at 945 °C for 10 s. The calculated atomic profiles for both the implanted S and N are also shown.

electron concentration in this thin layer is clearly attributable to the presence of N. The large reduction of the electron concentration in the (S+N) sample in the As-rich region at about 0.1 μm below the surface could also be related to a reduced availability of group V sites and an increased V_{Ga} concentration in this region [37]. The effect is exacerbated in the (S+N) sample where both S and N compete for the same group V element sites.

As shown previously, the much higher activation efficiency of group VI donors in GaN_xAs_{1-x} is the direct result of N-induced modifications [36, 37]. Considering both the band-gap energy reduction and the large enhancement of the electron effective mass, the high n_{max} in the near-surface region of the (S+N) sample ($\sim 1.5 \times 10^{19}$ cm^{-3}) implies that the N content in this thin near-surface nitride layer is $x = 0.0032$. This value is in good agreement with the calculated N concentration in this surface region ($x \approx 0.003$–0.01). With this N content the conduction band edge is shifted downward by 77 meV and the conduction band effective mass at the Fermi energy is ~3 times higher than that of GaAs [28].

TEM study shows that in addition to the commonly observed implantation-induced defects in both the S and S+N-implanted samples, a broad layer containing a high density of small voids (of an average size of about 4–5 nm), similar to those shown in figure 3, is observed in the S+N co-implanted sample. Most of these voids are concentrated in a layer extending from ~0.1 μm to ~0.3 μm below the surface. Their concentration abruptly faded outside this area. The location of these voids correlates very well with the region of reduced electron concentration measured by ECV shown in figure 12. We assume that these voids are formed as agglomerates of vacancies filled with N and act as defect centres compensating electrical activity of S donors.

Similar enhancement in the maximum free electron concentration near the surface is also obtained for Se and N co-implantation in GaAs. Figure 13 shows ECV results for Se- and Se+N-implanted GaAs after RTA at 945 °C for 10 s. Similar to the N+S results in figure 12, a very thin layer (~200 Å) with high electron concentration (up to 10^{19} cm^{-3}) was observed in the Se+N sample indicating the formation of a highly doped GaN_xAs_{1-x} layer.

In contrast to the successful formation of a GaN_xAs_{1-x} layer with electron concentration exceeding that of GaAs formed by group VI elements (S, Se) and N co-implantation, Si and N co-implantation in GaAs (with atomic profiles similar to the S and N co-implantation case) only resulted in a highly resistive layer. ECV profiling was carried out on a N+Si-implanted GaAs sample with N profile (~1% for 1000 Å) shallower than the Si profile ($\sim 3.6 \times 10^{20}$ cm^{-3} for the top ~0.2 μm) and the results are shown in figure 14. A comparison of the electron concentration profiles of the Si only and Si+N-implanted GaAs samples shows that a uniform layer with electron concentration of $\sim 2 \times 10^{18}$ cm^{-3} was obtained for the GaAs sample implanted with Si only. However, when N was co-implanted with Si, the top 1000 Å was depleted and no net ionized donor could be observed. Free electrons can be measured only beyond the N-implanted region, and this coincides with the electron concentration in the tail region of the Si only sample. This is most probably the result of a high tendency for the implanted Si and N atoms to form silicon nitride precipitates during post-implantation annealing, thus deactivating the Si donors in the Ga sublattice sites.

The large enhancement of electrical activation in a near-surface nitride layer observed in the S+N (as well as Se+N) implanted GaAs samples will be particularly useful in the fabrication of low resistivity, non-alloyed ohmic

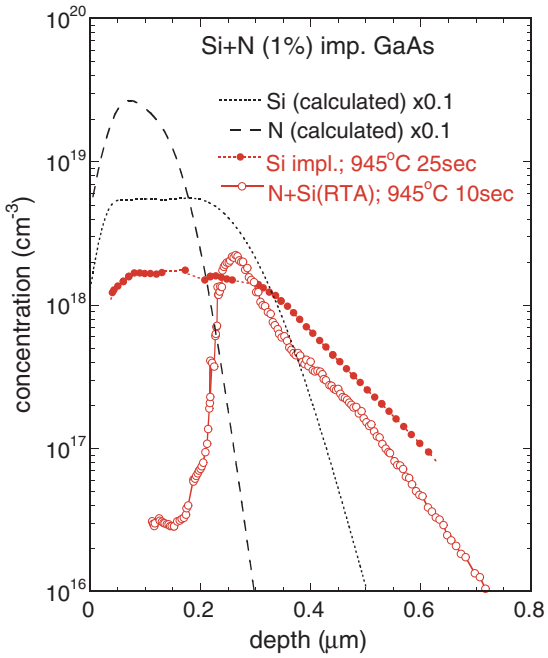

Figure 14. The ECV measured net donor concentration profiles for the GaAs samples implanted with Si alone and Si+N after RTA at 945 °C for 10 s. The calculated atomic profiles for both the implanted S and N are also shown. The N-implantation in this case is shallower than those in figures 15 and 16 and is only ∼1% for the top 1000 Å.

contacts to n-type GaAs. The current standard non-alloyed ohmic contacts to n-GaAs utilize either multi-component metallization [58, 59] e.g. MoGeInW, MoGeW, NiInW or heteroepitaxial structures such as graded $In_xGa_{1-x}As$ [60]. The minimum resistance of the multi-component contacts is still limited by the near-surface doping level and the graded contacts can be fabricated only through an epitaxial growth process.

The resistance of the ohmic contacts depends on the concentration of uncompensated donors in the near-surface region and the Schottky barrier heights, V_b. Our current results of ∼77 meV reduction in V_b and a high $n \approx 1.5 \times 10^{19}$ cm^{-3} in the S+N co-implanted GaAs sample will lead us to an almost two orders of magnitude reduction of the contact resistance for standard non-alloyed ohmic contacts. The idea of exploiting the exceedingly high free electron concentration that can be achieved in GaN_xAs_{1-x} thin films for the fabrication of low resistivity non-alloyed ohmic contacts has been explored recently [49]. Specific contact resistance of the order of $\sim 10^{-4}$ Ω cm^2 was achieved for a Au/GaAsNSe structure with an electron concentration of $\sim 10^{20}$ cm^{-3}.

3. Summary

Nitrogen implantation followed by rapid thermal processing was proved to be a practical and convenient method for the formation of diluted III–N_x–V_{1-x} alloys with strong N-induced modifications in the conduction band structure. Thin films of GaN_xAs_{1-x}, InN_xP_{1-x} and $Al_yGa_{1-y}N_xAs_{1-x}$ were synthesized by N$^+$-implantation into GaAs, InP and $Al_yGa_{1-y}As$. In all three cases the fundamental band gap energy for the ion beam synthesized III–N_x–V_{1-x} alloys was found to decrease with increasing N-implantation dose in a manner similar to that observed in epitaxially grown GaN_xAs_{1-x} thin films. The band-gap reductions in these N$^+$-synthesized III–N_x–V_{1-x} alloys can be quantitatively described by the band anticrossing model. In GaN_xAs_{1-x} the highest value of x (fraction of 'active' substitutional N on As sublattice) achieved using a conventional RTA technique was 0.006. It was observed that N_{As} is thermally unstable at temperatures higher than 850 °C. Using pulsed laser melting followed by RTA on the N$^+$-implanted GaAs samples, thermally stable GaN_xAs_{1-x} thin films with N content of the order of 1% with a fundamental band gap of 1.26 eV were obtained. The N activation efficiency in pulsed laser annealed GaN_xAs_{1-x} thin films is as much as a factor of 5 higher than that in GaN_xAs_{1-x} thin films synthesized by N$^+$-implantation and RTA only.

The highest value of x achieved in InN_xP_{1-x} was higher, 0.012, and the N_P was found to be stable to at least 850 °C. In addition, the N activation efficiency in implanted InN_xP_{1-x} was at least a factor of 2 higher than that in GaN_xAs_{1-x} under similar processing conditions. $Al_yGa_{1-y}N_xAs_{1-x}$ had not been made previously by epitaxial techniques. N$^+$-implantation was successful in producing $Al_yGa_{1-y}N_xAs_{1-x}$ alloys. Notably, the band gap of these alloys remains direct, even above the value of y ($y > 0.44$) where the band gap of the host material is indirect.

Maximum free electron concentration as high as 7×10^{19} cm^{-3} has been observed in heavily Se-doped $Ga_{1-3x}In_{3x}N_xAs_{1-x}$ ($x = 0.033$) films. This is more than 20 times larger than that observed in GaAs films grown under similar conditions. It is shown that the dramatic increase in the maximum free electron concentration is caused by a combination of two effects: (1) a downward shift of the conduction band and (2) an increase of the electron effective mass caused by flattening of the conduction band dispersion. Both these effects are due to modifications to the conduction band structure caused by an anticrossing interaction of a localized N state and the conduction band of the III–V host. Similar free electron concentration enhancement was also observed in a S-implanted MOCVD-grown GaN_xAs_{1-x} thin film.

Combining the ion synthesis of diluted nitrides and S-implantation doping techniques, we realized a large increase in the electrical activation of sulfur co-implanted with nitrogen in GaAs within a thin (<500 Å) near-surface region. A free electron concentration as high as 1.5×10^{19} cm^{-3} was observed in this layer, a factor of 5 higher than that in a GaAs sample implanted with S only. The high free electron concentration in this thin layer is the result of the incorporation of N on the As site which forms a thin diluted GaN_xAs_{1-x} alloy layer (∼500 Å) with $x \sim 0.3\%$. The results have important practical implications on the fabrication of low-resistance, non-alloyed ohmic contacts to n-type GaAs.

Acknowledgments

The author acknowledges the collaboration of W Walukiewicz, W Shan, J Wu, J W Beeman, J Jasinski, J W Ager III and E E Haller at LBNL, J F Geisz, D J Friedman and

J M Olson at NREL, H P Xin and C W Tu at UC SanDiego, M A Scarpulla and O D Dubon at UC Berkeley, M R Pillai and M J Aziz at Harvard University, and M C Ridgway at the Australian National University. This work was supported by the 'Photovoltaic Materials Focus Area' in the DOE Center of Excellence for the Synthesis and Processing of Advanced Materials, Office of Science, Office of Basic Energy Science and Division of Materials Sciences and Engineering of the US Department of Energy under contract No DE-AC03-76SF00098.

References

[1] Sakai S, Ueta Y and Terauchi Y 1993 *Japan. J. Appl. Phys.* **32** 4413
[2] Kondow M, Uomi K, Hosomi K and Mozume T 1994 *Japan. J. Appl. Phys.* **33** L1056
[3] Uesugi K, Morooka N and Suemune I 1999 *Appl. Phys. Lett.* **74** 1254
[4] Geisz J F, Friedman D J, Olson J M, Kurtz S R and Keyes B M 1998 *J. Cryst. Growth* **195** 401
[5] Baillargeon J N, Cheng K Y, Hofler G E, Pearah P J and Hsieh K C 1992 *Appl. Phys. Lett.* **60** 2540
[6] Shan W, Walukiewicz W, Yu K M, Wu J, Ager J W, Haller E E, Xin H P and Tu C W 2000 *Appl. Phys. Lett.* **76** 3251
[7] Bi W G and Tu C W 1996 *J. Appl. Phys.* **80** 1934
[8] Shan W, Walukiewicz W, Yu K M, Ager J W III, Haller E E, Geisz J F, Friedman D J, Olson J M, Kurtz Sarah R and Nauka K 2000 *Phys. Rev.* B **62** 4211
[9] Shan W, Yu K M, Walukiewicz W, Ager J W, Haller E E and Ridgway M C 1999 *Appl. Phys. Lett.* **75** 1410
[10] Kondow M, Kitatani T, Nakatsuka S, Larson M C, Nakahara K, Yazawa Y, Okai M and Uomi K 1997 *IEEE J. Sel. Top. Quantum Electron.* **3** 719
[11] Kondow M, Kitatani T, Larson M C, Nakahara K, Uomi K and Inoue H 1998 *J. Cryst. Growth* **188** 255
[12] Friedman D J, Geisz J F, Kurtz S R, Myers D and Olson J M 1998 *J. Cryst. Growth* **195** 409
[13] Kurtz S R, Allerman A A, Jones E D, Gee J M, Banas J J and Hammons B E 1999 *Appl. Phys. Lett.* **74** 729
[14] Shan W, Walukiewicz W, Ager J W III, Haller E E, Geisz J F, Friedman D J, Olson J M and Kurtz S R 1999 *Phys. Rev. Lett.* **82** 1221
[15] Perkins J D, Masceranhas A, Zhang Y, Geisz J F, Friedman D J, Olson J M and Kurtz S R 1999 *Phys. Rev. Lett.* **82** 3312
[16] Perlin P, Wisniewski P, Skierbiszewski C, Suski T, Kaminska E, Subramanya S G, Weber E R, Mars D E and Walukiewicz W 2000 *Appl. Phys. Lett.* **76** 1279
[17] Walukiewicz W, Shan W, Ager J W III, Chamberlin D R, Haller E E, Geisz J F, Friedman D J, Olson J M and Kurtz S R 1999 *Photovoltaics for the 21st Century* ed V K Kapur, R D McDonnell, D Carlson, G P Ceasar and A Rohatgi (Pennington: Electrochemical Society) p 190
[18] Shan W, Walukiewicz W, Ager J W III, Haller E E, Geisz J F, Friedman D J, Olson J M and Kurtz Sarah R 1999 *J. Appl. Phys.* **86** 2349
[19] Shan W, Walukiewicz W, Yu K M, Ager J W III, Haller E E, Xin H P and Tu C W 2000 *Appl. Phys. Lett.* **76** 3251
[20] Yu K M, Walukiewicz W, Shan W, Wu J, Beeman J W, Ager J W III, Haller E E, Xin H P and Tu C W 2001 *Appl. Phys. Lett.* **78** 1077
[21] Wolford D J, Bradley J A, Fry K and Thompson J 1984 *Proc. 17th Int. Conf. on the Physics of Semiconductors* ed J D Chadi and W A Harrison (New York: Springer) p 627
[22] Hung W K, Chern M Y, Fan J C, Lin T Y and Chen Y F 1999 *Appl. Phys. Lett.* **74** 3951
[23] Hung W K, Chern M Y and Chen Y F 2000 *Semicond. Sci. Technol.* **15** 892
[24] Yu K M, Walukiewicz W, Shan W, Wu J, Beeman J, Ager J W III, Haller E E and Ridgway M C 2001 *Mater. Res. Soc. Symp. Proc.* **647** O13.3.1/R8.3.1
[25] Yu K M, Walukiewicz W, Wu J, Beeman J W, Ager J W III, Haller E E, Shan W, Xin H P, Tu C W and Ridgway M C 2001 *J. Appl. Phys.* **90** 2227
[26] Jasinski J, Yu K M, Walukiewicz W, Liliental-Weber Z and Washburn J 2001 *Appl. Phys. Lett.* **79** 931
[27] Jasinski J, Yu K M, Walukiewicz W, Liliental-Weber Z and Washburn J 2001 *Presented at the 21st Int. Conf. on Defects in Semiconductors (ICDS21) (16–20 July 2001, Giessen, Germany)*
[28] Skierbiszewski C *et al* 2000 *Appl. Phys. Lett.* **76** 2409
[29] Laks D B, Van de Walle C G, Neumark G F and Pantelides S T 1991 *Phys. Rev. Lett.* **66** 648
[30] Chadi D J 1994 *Phys. Rev. Lett.* **72** 534
[31] Garcia A and Northrup H 1995 *Phys. Rev. Lett.* **74** 1131
[32] Saarinen K, Nissilä J, Kauppinen H, Hakala M, Puska M J, Hautojärvi P and Corbel C 1999 *Phys. Rev. Lett.* **82** 1883
[33] Walukiewicz W 1989 *Appl. Phys. Lett.* **54** 2094
[34] Walukiewicz W 1993 *Mater. Res. Soc. Symp. Proc.* **300** 421
[35] Walukiewicz W 1993 *Proc. 17th Int. Conf. on Defects in Semicon., Mats. Science Forum* vol 143–147 p 519
[36] Yu K M, Walukiewicz W, Shan W, Ager J W III, Wu J, Haller E E, Geisz J F, Friedman D J, Olson J M and Kurtz Sarah R 2000 *Phys. Rev.* B **61** R13337
[37] Yu K M, Walukiewicz W, Shan W, Wu J, Ager J W III, Haller E E, Geisz J F and Ridgway M C 2000 *Appl. Phys. Lett.* **77** 2858
[38] Yu K M, Walukiewicz W, Shan W, Wu J, Beeman J W, Ager J W III and Haller E E 2000 *Appl. Phys. Lett.* **77** 3607
[39] Aspnes D E 1973 *Surf. Sci.* **37** 418
[40] Heckingbottom R and Ambridge T 1973 *Radiat. Eff.* **17** 31
[41] Moll J, Yu Kin Man, Walukiewicz W, Hansen W L and Haller E E 1992 *Appl. Phys. Lett.* **60** 2383
[42] Kringhøj P 1994 *Appl. Phys. Lett.* **64** 351
[43] Yu Kin Man and Ridgway M C 1998 *Appl. Phys. Lett.* **73** 52
[44] Yu K M, Walukiewicz W, Beeman J W, Scarpulla M A, Dubon O D, Pillai M R and Aziz M 2002 *Appl. Phys. Lett.* **80** 3958
[45] Makita Y, Ijuin H and Gonda S 1976 *Appl. Phys. Lett.* **28** 287
[46] Gonda S and Makita Y 1975 *Appl. Phys. Lett.* **27** 392
[47] Hjalmarson H P, Vogl P, Wolford D J and Dow J D 1980 *Phys. Rev. Lett.* **44** 810
[48] Geisz J F, Friedman D J, Olson J M, Kurtz S R and Keyes B M 1998 *J. Cryst. Growth* **195** 401
[49] Uesugi Katsuhiro and Suemune Ikuo 2001 *Appl. Phys. Lett.* **79** 3284
[50] Christel L A and Gibbons J F 1981 *J. Appl. Phys.* **52** 5050
[51] Yeo Y K, Park Y S and Kwor P 1982 *J. Appl. Phys.* **53** 1815
[52] Kwor P, Yeo Y K and Park Y S 1982 *J. Appl. Phys.* **53** 4786
[53] Kuzuhara M, Kohzu H and Takayama Y 1983 *J. Appl. Phys.* **54** 3121
[54] Pertritz R L 1958 *Phys. Rev.* **110** 1254
[55] Wang Kou-Wei 1987 *Appl. Phys. Lett.* **51** 2127
[56] Rao Mulpuri V and Nadella Ravi K 1990 *J. Appl. Phys.* **67** 1761
[57] Yu Kin Man and Ridgway M C 2000 *Nucl. Instrum. Methods* B **168** 65
[58] Murakami M and Price W H 1987 *Appl. Phys. Lett.* **51** 664
[59] Murakami M, Price W H, Shih T-C, Childs K D, Furman B K and Tiwari S 1987 *J. Appl. Phys.* **62** 3288
[60] DiLorenzo J V, Niehaus W C and Cho A Y 1979 *J. Appl. Phys.* **50** 951